Fluctuating Hydrodynamics and Direct Simulation Monte Carlo

Kaushik Balakrishnan*, John B. Bell*, Aleksandar Donev† and Alejandro L. Garcia**

*Center for Computational Science and Engineering, Lawrence Berkeley Nat. Lab., Berkeley, CA, 94720
†Courant Institute of Mathematical Sciences, New York University, NY 10012
**Department of Physics and Astronomy, San Jose State University, San Jose, California, 95192

Abstract. Thermodynamic fluctuations are significant at microscopic scales even when hydrodynamic transport models (i.e., Navier-Stokes equations) are still accurate; a well-known example is Rayleigh scattering, which makes the sky blue. Interesting phenomena also appear in non-equilibrium systems, such as the enhancement of diffusion during mixing due to the correlation of velocity and concentration fluctuations. Direct Simulation Monte Carlo (DSMC) simulations are useful in the study of hydrodynamic fluctuations due to their computational efficiency and ability to model molecular detail, such as internal energy and chemical reactions. More recently, finite volume schemes based on the fluctuating hydrodynamic equations of Landau and Lifshitz have been formulated and validated by comparisons with DSMC simulations. This paper discusses some of the relevant numerical issues and physical effects investigated using DSMC and stochastic Navier-Stokes simulations. This paper also presents the multi-component fluctuating hydrodynamic equations, including chemical reactions, and illustrates their numerical solutions in the study of Turing patterns. We find that behind a propagating reaction front, labyrinth patterns are produced due to the coupling of reactions and species diffusion. In general, fluctuations accelerate the propagation speed of the leading front but differences are observed in the Turing patterns depending on the origin of the fluctuations (stochastic hydrodynamic fluxes versus Langevin chemistry).

Keywords: Thermal fluctuations, DSMC, Turing instability, Reaction-diffusion systems
PACS: 82.20.–w, 47.54.Bd, 47.51.+a

INTRODUCTION

Science and engineering are increasingly operating at the micro- and nano-scales to achieve objectives at the macro-scale. Many important physical and chemical processes occur across this range of time and length scales, for example: nucleation and phase separation; combustion and ignition; fluid instabilities; and surface science, such as catalytic processes.

All devices that operate at molecular scales, from microelectromechanical systems (MEMS) to natural biomolecules, function in chaotic conditions due to thermal fluctuations. It is well-known that hydrodynamic fluctuations play an important role in the Brownian motion of suspended microscopic objects but other examples include: the breakup of droplets in jets [1]; Brownian molecular motors [2], Rayleigh-Bernard convection [3]; Rayleigh-Taylor mixing [4]; and, combustion and explosive detonation [5]. Fluctuations also alter pattern formations in reaction-diffusion systems [6, 7, 8].

This increasing interest in micro- and nano-fluidics has necessitated the development of numerical schemes for hydrodynamic calculations at the molecular scale. [9, 10] Direct Simulation Monte Carlo (DSMC) [11] was developed to model gas flows in which the Knudsen number (ratio of mean free path to system length) is large and the original applications were rarefied gas flows in which transport properties are not well-approximated by the Navier-Stokes equations. Since the early 90's DSMC has also been used in modeling molecular-scale devices with system lengths of microns down to nanometers (e.g., [12, 13]). Thanks to its excellent computational efficiency, DSMC is also an ideal particle-based scheme for the study of hydrodynamic fluctuations.

Surprisingly, it also turns out that hydrodynamic transport models are often still accurate at the microscopic scales for which thermodynamic fluctuations are significant. Specifically, the fluctuating Navier-Stokes (FNS) equations, introduced by Landau and Lifshitz, have been validated by laboratory experiments (e.g., light scattering) and molecular simulations. [14, 15] Recently, efficient and accurate Langevin-type schemes have been developed for the FNS equations. [16, 17]

This paper discusses the study of hydrodynamic fluctuations using DSMC and FNS solvers, highlighting some numerical issues and physical effects investigated using these two methods. We also present the multi-component fluctuating reacting hydrodynamic equations and illustrate their use in the study of Turing patterns.

HYDRODYNAMIC FLUCTUATIONS – NUMERICAL ISSUES

As with all particle-based schemes, DSMC requires statistical averaging to measure hydrodynamic values. The confidence intervals for these measured values can be estimated from the variances of equilibrium fluctuations (see [18] and Plotnikov and Shkarupa's contribution in this volume). For example, the fractional error in the fluid velocity goes as $(\mathrm{Ma}\sqrt{SN})^{-1}$ where S is the number of independent samples, N is the number of particles, and Ma is the Mach number. From this result we see that for a given fractional error the required number of samples goes as Ma^{-2}. Consequently, low-speed flows, such as those in nano-fluidic devices, require expensive DSMC computations to resolve the mean values of hydrodynamic quantities. This difficulty has motivated low-variance deviational methods, as described in Hadjiconstantinou's contribution in this volume. Note that the fluctuations in DSMC match those in the physical system if the ratio of physical molecules represented per DSMC particle is 1:1, otherwise the variances of the fluctuations in DSMC are magnified by the value of this ratio. [18]

A more subtle numerical issue arises from the correlation of fluctuations. At equilibrium, fluctuations of conjugate hydrodynamic quantities are uncorrelated (e.g., density is uncorrelated with fluid velocity and temperature). However, these quantities are correlated out of equilibrium and these correlations can introduce a statistical bias when estimating hydrodynamic quantities in particle-based simulations such as DSMC. As a specific example, one can measure the instantaneous fluid velocity as, $\mathbf{u} = N^{-1}\sum_i^N \mathbf{v}_i$ where the sum over particles in a sampling cell. The mean value of instantaneous fluid velocity, estimated from S samples, is

$$\langle \mathbf{u} \rangle = \frac{1}{S}\sum_{j=1}^{S} \mathbf{u}(t_j) = \frac{1}{S}\sum_{j=1}^{S}\left(\frac{1}{N(t_j)}\sum_{i\in C}^{N(t_j)} \mathbf{v}_i(t_j)\right).$$

An alternative definition for average fluid velocity often used in DSMC is the cumulative average,

$$\langle \mathbf{u} \rangle_* = \frac{\sum_{j=1}^{S}\sum_{i\in C}^{N(t_j)} \mathbf{v}_i(t_j)}{\sum_{j=1}^{S} N(t_j)}.$$

These two expressions for fluid velocity can be written as, $\langle \mathbf{u} \rangle = \langle \mathbf{J}/M \rangle$ and $\langle \mathbf{u} \rangle_* = \langle \mathbf{J} \rangle / \langle M \rangle$ where M, and J are the total mass and momentum of particles in the sampling cell. Due to the correlation of fluctuations these two expressions, in general, give different results and the cumulative average, $\langle \mathbf{u} \rangle_*$, yields the correct hydrodynamic value; specifically, the statistical bias is $\langle \mathbf{u} \rangle - \langle \mathbf{u} \rangle_* \approx -\langle \delta\rho\,\delta\mathbf{u} \rangle / \langle \rho \rangle$. [19] The mean value of instantaneous temperature has a similar bias that goes as $\langle \delta\rho\,\delta T \rangle / \langle \rho \rangle$; since this statistical bias is $O(N^{-1})$ the mean value of instantaneous temperature is *not* an intensive quantity. For details, see [20].

Finally, in some scenarios DSMC lacks the computational efficiency necessary to study problems in which very large numbers of particles are needed to fill the required computational domain. In this regard hybrid methods are useful since a particle method can be used in regions where the continuum description fails or is difficult to implement, and a more efficient continuum description can be used elsewhere. [21, 22] However, fluctuations in the particle region of a hybrid are suppressed by the coupling to a deterministic continuum PDE solver. [23, 24] This deficiency can be corrected by using a stochastic hydrodynamic scheme based on the FNS equations. [17, 25],

HYDRODYNAMIC FLUCTUATIONS – PHYSICAL EFFECTS

Thermal fluctuations in non-equilibrium systems with a constant imposed gradient exhibit interesting behavior, such as long-range correlations between fluctuations. [15] This phenomenon is well-known and theoretical predictions from fluctuating hydrodynamic theory are found to be in excellent agreement with correlations measured in DSMC simulations. [26, 27]

A related phenomena recently investigated by DSMC simulations is the effect of thermal velocity fluctuations on the effective diffusion coefficient in a binary mixture of distinguishable, identical fluids. [28, 29]. Recent laboratory experiments have demonstrated that the length scale for concentration fluctuations during mixing can grow to macroscopic

(millimeter) size due to the correlation of species density and species velocity fluctuations. Fluctuating hydrodynamic theory that predicts this correlation, in Fourier space, goes as $(k_\perp^2/k^4)\nabla c$, which is verified by DSMC simulations (see Figure 1).

The steady-state diffusive flux in a finite system subject to a concentration gradient is enhanced because of this long-range correlation between concentration fluctuations and fluctuations of the velocity parallel to the concentration gradient. A simple fluctuating hydrodynamics theory, closely related to second-order mode-mode coupling analysis, predicts that the enhancement of diffusive transport depends on the system width L perpendicular to the imposed gradient. Specifically, the enhancement $\Delta D \propto \ln(L/L_0)$ in quasi-two-dimensional systems, while in three dimensions it goes as $L_0^{-1} - L^{-1}$, where L_0 is a reference length. The predictions are in excellent agreement with numerical solutions of the full fluctuating Navier-Stokes equations and with measurements from DSMC simulations (see Fig. 1).

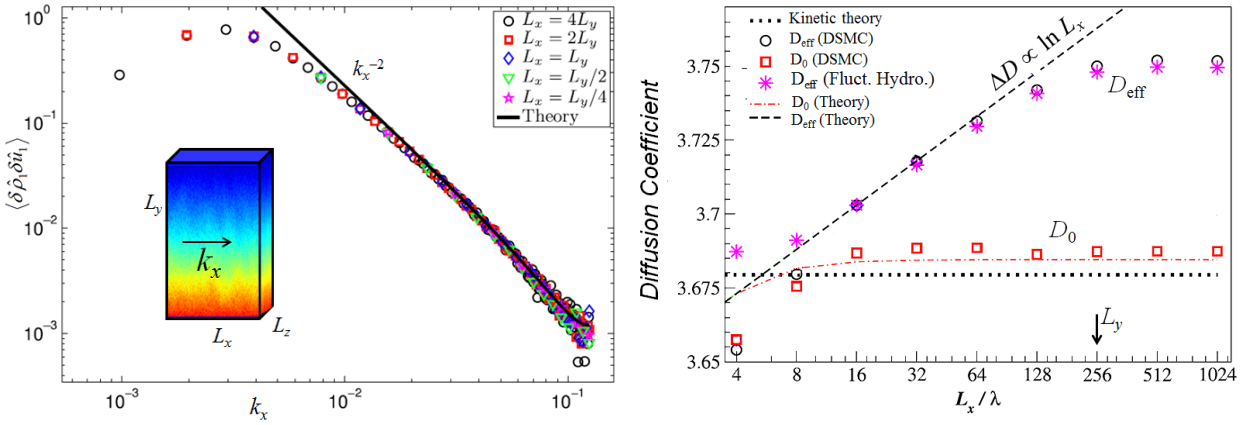

FIGURE 1. (Left) Discrete structure factor for species density and velocity fluctuations measured in DSMC simulations (markers) and predicted by fluctuating hydrodynamic theory (line). (Right) The effective and renormalized diffusion coefficients, $D_{\rm eff}$ and D_0, as functions of system width predicted by fluctuating hydrodynamic theory (lines) and measured in both DSMC simulations and numerical FNS calculations (markers).

HYDRODYNAMIC FLUCTUATIONS AND CHEMISTRY

The phenomena discussed in the sections above are present in simple gases, such as hard spheres. Realistic gases introduce additional physical effects, such as: complex transport properties (e.g., Soret effect); internal degrees of freedom; disassociation, recombination, and chemistry. Both DSMC and fluctuating hydrodynamic theory become more complicated but interesting new phenomena appear (see, for example, the contribution by Lemarchand and Nowakowski in these proceedings).

This section summarizes the formulation of the multi-component, reacting Fluctuating Navier-Stokes (FNS) equations. Specifically, the multi-component Navier-Stokes equations for dilute gases [30] are extended to also include stochastic flux terms. The continuity, species, momentum and energy equations for FNS are:

$$\frac{\partial}{\partial t}(\rho) + \nabla\cdot(\rho\mathbf{u}) = 0, \tag{1}$$

$$\frac{\partial}{\partial t}(\rho Y_k) + \nabla\cdot(\rho\mathbf{u}Y_k) + \nabla\cdot\left[\mathbf{F_k} + \widetilde{\mathbf{F_k}}\right] = \Omega_k + \widetilde{\Omega_k}, \tag{2}$$

$$\frac{\partial}{\partial t}(\rho\mathbf{u}) + \nabla\cdot(\rho\mathbf{u}\otimes\mathbf{u}) + \nabla p + \nabla\cdot\left[\Pi + \widetilde{\Pi}\right] = \rho\mathbf{g}, \tag{3}$$

$$\frac{\partial}{\partial t}(\rho E) + \nabla\cdot(\rho\mathbf{u}E + p\mathbf{u}) + \nabla\cdot\left[\mathbf{Q} + \widetilde{\mathbf{Q}}\right] + \nabla\cdot\left(\left[\Pi + \widetilde{\Pi}\right]\cdot\mathbf{u}\right) = \rho\mathbf{u}\cdot\mathbf{g}, \tag{4}$$

where ρ, $\mathbf{u}$, T and p denote the density, fluid velocity, temperature and pressure, respectively, of the mixture. The mass fraction of the k-th species is given by Y_k, with $\sum_{k=1}^{N_s} Y_k = 1$, where N_s is the total number of species in the system. For an ideal gas mixture we can explicitly write the mechanical equation of state,

$$p = \rho R_u T \sum_{k=1}^{N_s} \frac{Y_k}{W_k}. \tag{5}$$

The universal gas constant is $R_u = k_B N_A$, where k_B is Boltzmann's constant and N_A is Avogadro's number; the molecular weight of the k-th species is $W_k = m_k N_A$ where m_k is the mass of a molecule of that species. The total specific energy is given by $E = e(\rho, T, Y_k) + \frac{1}{2}|\mathbf{u}|^2$. with the thermal equation of state,

$$e(T, Y_k) = \sum_{k=1}^{N_s} Y_k e_k(T), \qquad \text{and} \qquad h(T, Y_k) = \sum_{k=1}^{N_s} Y_k h_k(T), \tag{6}$$

where e_k and h_k are the specific internal energy and enthalpy of the k-th species with $h_k = e_k + R_u T/W_k$. The terms on the right hand sides of eqs. (3) and (4) are due to a body force, such as gravity, with acceleration $\mathbf{g}$.

The viscous stress tensor is Π and, under the Newtonian assumption, is given by:

$$\Pi_{ij} = -\eta \left(\frac{\partial u_i}{\partial x_j} + \frac{\partial u_j}{\partial x_i} \right) - \delta_{ij} \left(\xi - \frac{2}{3}\eta \right) \sum_k \frac{\partial u_k}{\partial x_k}, \tag{7}$$

where δ_{ij} is the Kronecker delta, η is the coefficient of viscosity, and ξ is the coefficient of bulk viscosity. The vector $\mathbf{Q}$ is the heat flux and is given by,

$$\mathbf{Q} = \sum_{k=1}^{N_s} h_k \mathbf{F_k} - \lambda \nabla T + R_u T \sum_{k=1}^{N_s} \frac{\widehat{\chi_k}}{W_k} \mathbf{F_k}, \tag{8}$$

for an ideal gas. Here, λ is the thermal conductivity of the mixture, and $\widehat{\chi_k}$ are the rescaled thermal diffusion ratios.

The diffusion flux of the k-th species is given by $\mathbf{F_k}$ and is governed by Fick's law:

$$\mathbf{F_k} = -\sum_{l=1}^{N_s} \rho \widehat{D_{kl}} \left(\mathbf{d_l} + X_l \widehat{\chi_l} \frac{\nabla \mathbf{T}}{T} \right), \tag{9}$$

where $\widehat{D_{kl}}$ are the multi-component flux diffusion coefficients [31], $\mathbf{d_l}$ is the diffusion driving force of the l-th species. The expression for $\mathbf{d_l}$ is given by:

$$\mathbf{d_l} = \nabla X_l + (X_l - Y_l) \frac{\nabla p}{p}, \tag{10}$$

where X_l is the mole fraction of the l-th species and is related to Y_l as $X_l = Y_l \overline{W}/W_l$. Here, $\overline{W}$ is the mixture-averaged molecular weight and is obtained as

$$\frac{1}{\overline{W}} = \sum_{k=1}^{N_s} \frac{Y_k}{W_k}. \tag{11}$$

Finally, the source term Ω_k in Eq. (2) is the rate of production of the k-th species due to chemical reactions. For mass conservation, we require $\sum_{k=1}^{N_s} \Omega_k = 0$ and $\sum_{k=1}^{N_s} \mathbf{F_k} = 0$.

For a multi-component mixture, the fluid viscosity, η, and the thermal conductivity, λ, are determined using the expressions given in [32]. The flux diffusion coefficients, $\widehat{D_{kl}}$, are computed using the approximate expressions presented in [31] and from them $\widehat{\chi_k}$ can be evaluated using [33, 34]. Thus, all the transport coefficients are dependent only on the species mass fractions, molecular weights and their diameters. The important properties of $\widehat{D_{kl}}$ are that: $\widehat{D_{kl}}$ is not symmetric; for each column of $\widehat{D_{kl}}$, the row entries sum to zero; the diagonal entries of $\widehat{D_{kl}}$ are strictly positive.

The terms that appear with a tilde in the governing equations denote stochastic contributions, i.e., the effect of fluctuations at the micro-scales on the macro-scales. The stochastic viscous flux tensor is a Gaussian random field with covariance given by

$$\langle \widetilde{\Pi}\,,\, \widetilde{\Pi}^{*} \rangle = \left[2k_B\eta T \;\; (\delta_{ik}\delta_{jl} + \delta_{il}\delta_{jk}) + (2k_B T(\xi - 2/3\eta))\,\delta_{ij}\delta_{kl} \right] \delta(t-t')\delta(\mathbf{r}-\mathbf{r}'). \tag{12}$$

Discretization of the stochastic stress tensor in a form that maintains the correct fluctuation dissipation relation is somewhat delicate. See [17, 35] for details of the numerics. The stochastic heat flux is [17]

$$\widetilde{\mathbf{Q}} = \sqrt{2k_B\lambda T^2}\;\mathscr{W}^{(T)} + \sum_{k=1}^{N_s} \left(\frac{R_u T}{W_k}\widehat{\chi}_k + h_k \right) \widetilde{\mathbf{F}_\mathbf{k}}, \tag{13}$$

where $\mathscr{W}^{(T)}$ is a white noise random Gaussian vector with uncorrelated components,

$$\left\langle \mathscr{W}_i^{(T)}(\mathbf{r},t)\mathscr{W}_j^{(T)}(\mathbf{r}',t') \right\rangle = \delta_{ij}\delta(t-t')\delta(\mathbf{r}-\mathbf{r}'). \tag{14}$$

The stochastic diffusion flux of the k-th species is

$$\widetilde{\mathbf{F}_\mathbf{k}} = \sqrt{\frac{\rho}{N_A}} \sum_{l=1}^{N_s} \left(\sqrt{\widehat{D}A} \right)_{kl} \mathscr{W}^{(Y_l)}, \tag{15}$$

where we define the A matrix as, $A_{ij} = \overline{W} Y_i (2\delta_{ij} - 1)$. The matrix A satisfies the following conditions:

1. $\widehat{D}A$ is a symmetric, positive, semi-definite matrix.
2. For each column, the sum of the entries in each row of the $\sqrt{\widehat{D}A}$ matrix is zero. This condition is essential to conserve mass (see [30] for more details).
3. For a vanishing species concentration, say, $Y_k = 0$, the entire k-th row and k-th column of the $\sqrt{\widehat{D}A}$ matrix vanish and the system behaves as if the k-th species did not exist.

It may be shown that this form of the stochastic diffusion flux $\widetilde{\mathbf{F}_\mathbf{k}}$ is consistent with the GENERIC formulation of Ottinger [36], and thus satisfies a fluctuation-dissipation principle.

For the computation of the matrix square root, one can employ numerical iterative strategies. [37] Another option is to use Cholesky decomposition since $\widehat{D}A$ can be written as $\mathscr{L}\mathscr{L}^T$, where $\mathscr{L}$ is a lower triangular matrix, so that,

$$\widetilde{\mathbf{F}_\mathbf{k}} = \sqrt{\frac{\rho}{N_A}} \sum_{l=1}^{N_s} \mathscr{L}_{kl} \mathscr{W}^{(Y_l)}. \tag{16}$$

Computing the Cholesky decomposition can be relatively faster than numerically determining the matrix square root, particularly when the number of species involved is large. Thus, we recommend the use of Cholesky decomposition of $\widehat{D}A$ and then the use of Eq. (16) for the determination of $\widetilde{\mathbf{F}_\mathbf{k}}$.

To include chemical reactions we assume that the species, $\{\mathscr{S}_1, \ldots, \mathscr{S}_{N_s}\}$ participate in M_r reactions, represented as

$$\sum_{k=1}^{N_s} r_{k,l}\mathscr{S}_k \xrightarrow{K_l} \sum_{k=1}^{N_s} p_{k,l}\mathscr{S}_k, \qquad\qquad l = 1, ..., M_r. \tag{17}$$

where K_l is the reaction rate of the l-th reaction; note that reversible reactions are treated as two separate reactions. Following [38], the deterministic chemical reaction rates are given by

$$\Omega_k = \sum_{l=1}^{M_r} \nu_{k,l} W_k K_l \prod_{i=1}^{N_s} \left(\frac{\rho Y_i}{W_i} \right)^{r_{i,l}}, \tag{18}$$

where $\nu_{k,l} = p_{k,l} - r_{k,l}$ is the stoichiometric coefficient associated with species k in the l-th reaction.

Using a chemical Langevin model [39, 40, 41, 42], the stochastic chemical reaction rates are evaluated as

$$\widetilde{\Omega_k} = \sum_{l=1}^{M_r} \frac{\nu_{k,l} W_k}{\sqrt{N_A}} \sqrt{K_l \prod_{i=1}^{N_s} \left(\frac{\rho Y_i}{W_i} \right)^{r_{i,l}}}\, \mathscr{W}_l^{(R)}, \tag{19}$$

where N_A is the Avogadro number and $\mathscr{W}_l^{(R)}$ is is a white noise random Gaussian vector with uncorrelated components (similar to $\mathscr{W}^{(T)}$). Finally, the different stochastic fluxes are uncorrelated so $\langle \mathscr{W}^{(\alpha)}\mathscr{W}^{(\beta)} \rangle = 0$ if $\alpha \neq \beta$.

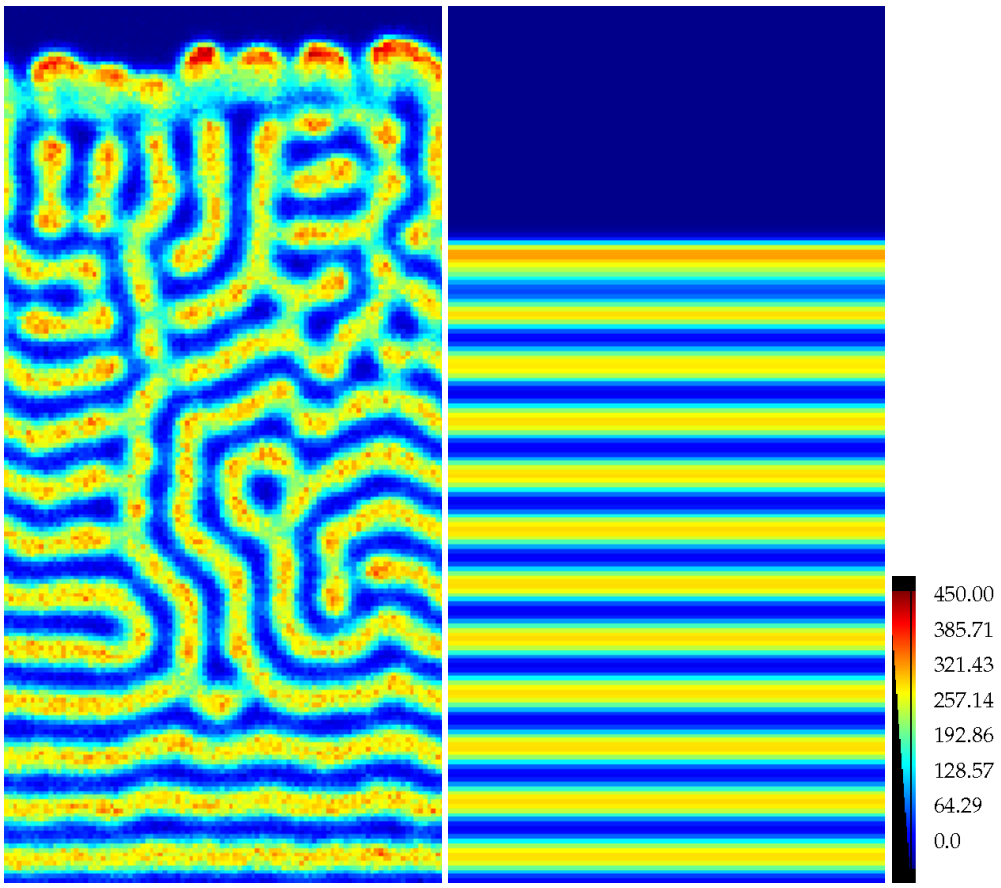

FIGURE 2. Number of species A particles per unit volume, $\rho Y_A/m_A$, for a Turing instability in a planar geometry: (Left, Case FF) Fluctuating hydrodynamics with fluctuating chemistry; (Right, Case DD) Deterministic hydrodynamics with deterministic chemistry.

NUMERICAL EXAMPLE: TURING PATTERNS

We demonstrate the fluctuating hydrodynamic reaction-diffusion formulation from the preceding section by applying it to the study of pattern formation resulting from the Turing instability [43]. Specifically, we investigate this instability using the Schlogl model [44], which has four species (A, B, C, D) and five reactions, summarized below:

$$A \overset{k_1}{\to} C, \qquad 2A + B \overset{k_2}{\to} 3A, \qquad B \overset{k_3}{\to} D, \qquad D \overset{k_4}{\to} B, \qquad D \overset{\text{at the rate of } \Omega_D}{\to} C. \tag{20}$$

Species D is taken as a reservoir species whose mass fraction is held fixed by setting the rate of the fifth reaction step so that Y_D is unaltered by chemistry.

The system admits homogeneous steady states (A_0, B_0, C_0, D_0), (A_+, B_+, C_+, D_+) and (A_-, B_-, C_-, D_-). (See [7, 8] for more details). Typically, a small region at the state '+', when exposed to a surrounding large region at state '0', gives rise to an evolving chemical wave front. In the wake of the front, Turing instability ensues, giving rise to labyrinth patterns.

In [7] it is demonstrated that internal fluctuations accelerate the formation of the Turing patterns, in a reaction-diffusion system without cross-diffusion. More recently, [8] carried out DSMC simulations of the same problem, albeit in one-dimension. Here we investigate the model using numerical simulations of the full hydrodynamic equations with chemistry, as described in the previous section; the numerics follow the general formulation described in [17] and the details, including comparisons with DSMC simulations, will be presented elsewhere [35].

The classical Schlogl front is generally simulated in a planar domain, as in [7, 8]; here we consider both planar and cylindrical geometries. The parameter values are summarized as follows. Particles of species (A, B, C, D)

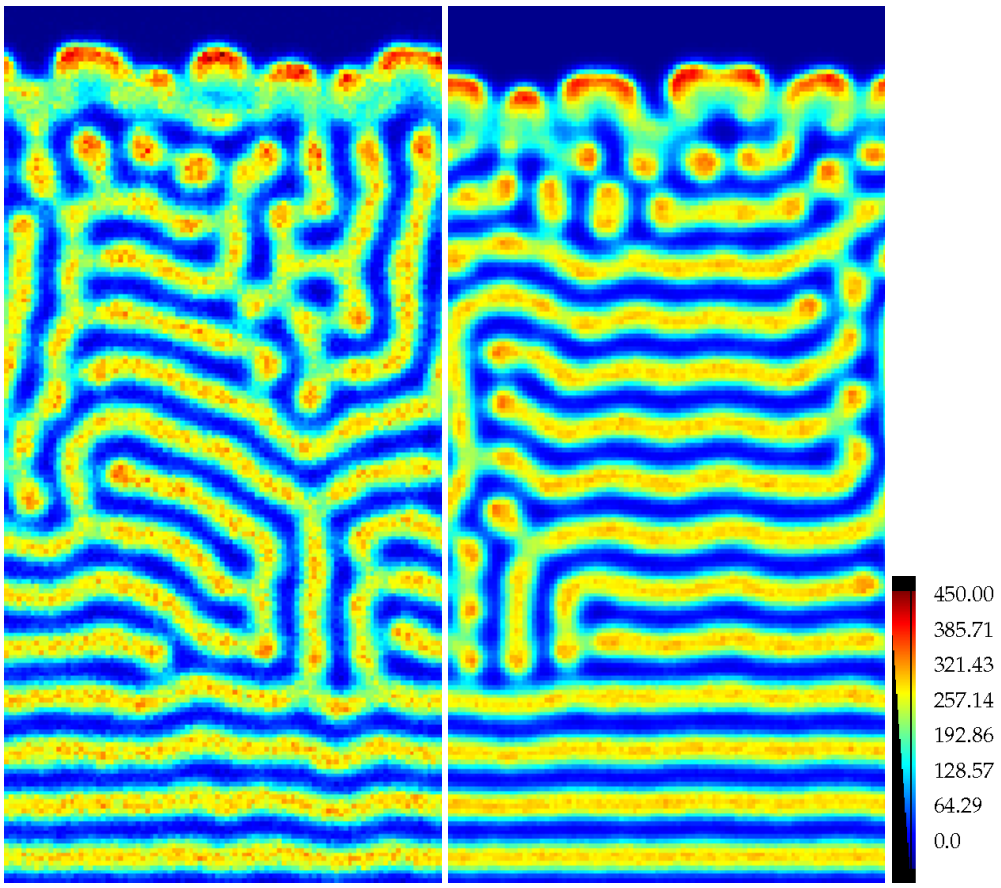

FIGURE 3. Number of species A particles per unit volume, $\rho Y_A/m_A$, for a Turing instability in a planar geometry: (Left, Case FD) Fluctuating hydrodynamics with deterministic chemistry; (Right, Case DF) Deterministic hydrodynamics with fluctuating chemistry.

have equal masses ($m_k = W_k = N_A = 1$) and diameters, $d_k = \left(0.05236, 2.686\times10^{-4}, 0.0238, 0.0238\right)$ with the hydrodynamic transport properties taken to be those of a hard sphere gas. The reaction rate constants are given by $k_l = \left(0.02567, 8.79\times10^{-7}, 0.01925, 0.013804\right)$. Species D's mass fraction is held fixed at $Y_D = 0.1$; any D that is consumed or produced during a time step is instantly transformed to C and the mass fraction of C is adjusted in every cell at every time step so as to ensure that the mass fractions of the four species sum to unity.[1] For these chosen parameters, the mass fractions corresponding to the '+' state are given by $(0.03129, 0.03006, 0.83865, 0.1)$ and state '0' as $(0, 0.07178, 0.82822, 0.1)$.

For the planar front, a $100\times200\times4$ grid is used with no-flux boundaries at the top and bottom, and periodic otherwise; the bottom 10 cells ($10\times200\times4$) are initialized with the '+' state, and the state '0' otherwise; thus, the reaction front propagates from the bottom to the top. For the cylindrical front, a $200\times200\times4$ grid is used with periodic boundaries everywhere; the '+' state is initialized in a central cylindrical region in the $x-y$ plane of radius equal to 5% of the total domain width in x or y, and the state '0' otherwise; thus, the reaction front propagates radially outwards. For all cases in both geometries the initial temperature, density, and pressure are $T = 1$ $\rho = 5578$, and $p = 5578$, with $k_B = 1$. The cell size dimensions are $\Delta x = \Delta y = \Delta z = 1$, and the time step is $\Delta t = 0.25$, which is about half of the maximum stable time step.[2]

---

[1] Note that only the mass fractions are altered and that the mass is still conserved since the species have equal molecular weights.
[2] For the parameters chosen is these simulations the limiting time scale is viscous dissipation.

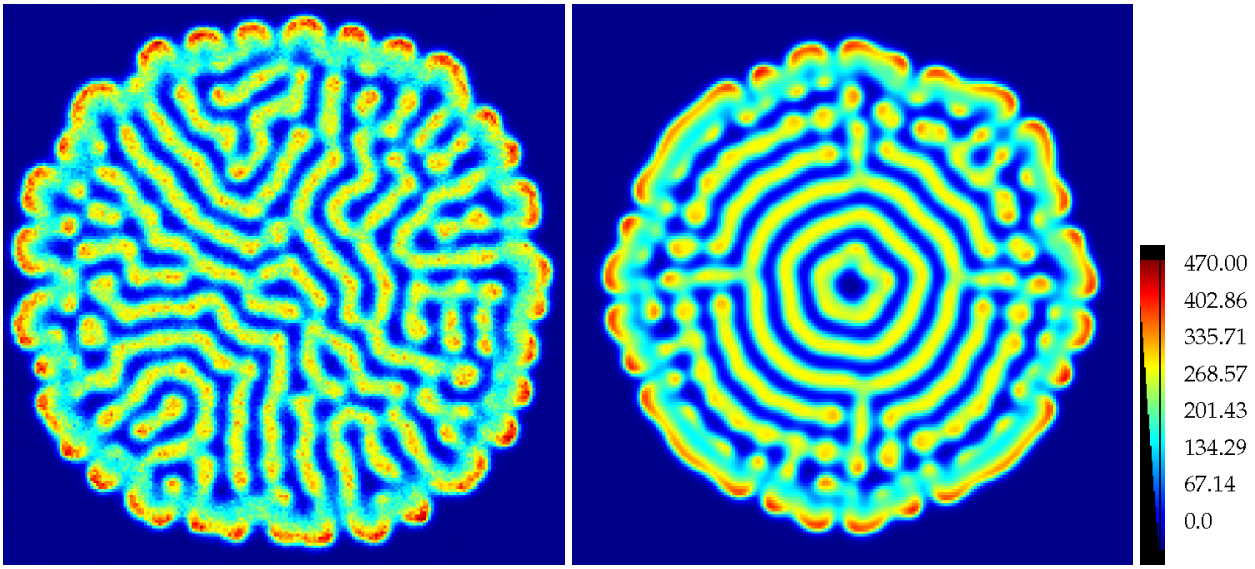

FIGURE 4. Number of species A particles per unit volume, $\rho Y_A/m_A$, for a Turing instability in a cylindrical geometry: (Left, Case FF) Fluctuating hydrodynamic equations with fluctuating chemistry; (Right, Case DD) Deterministic hydrodynamic equations with deterministic chemistry.

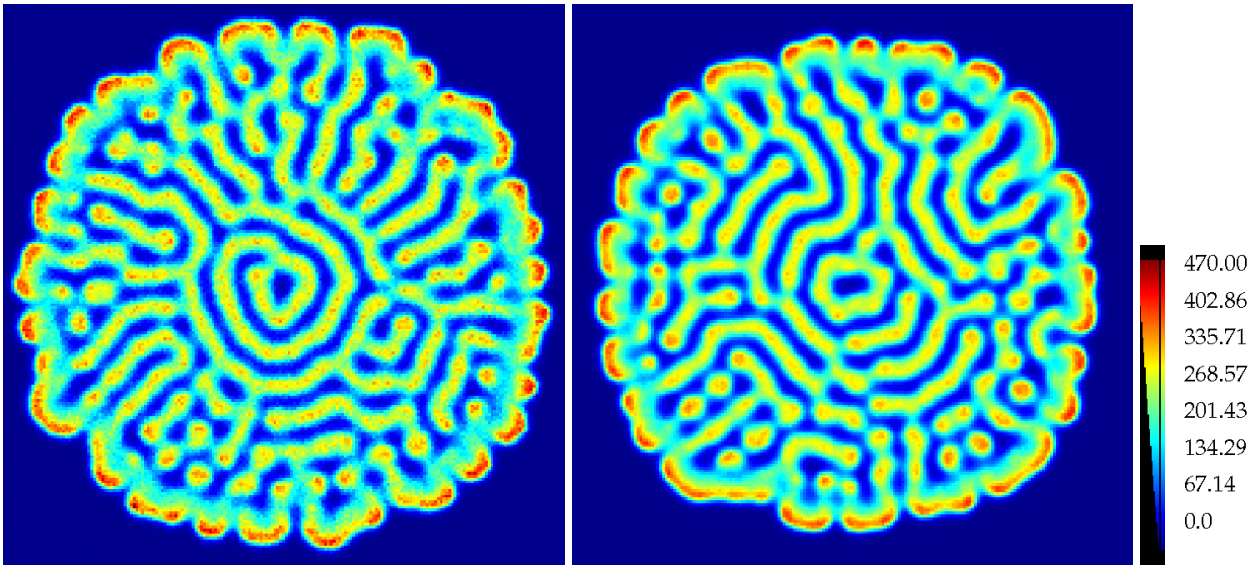

FIGURE 5. Number of species A particles per unit volume, $\rho Y_A/m_A$, for a Turing instability in a cylindrical geometry: (Left, Case FD) Fluctuating hydrodynamic equations with deterministic chemistry; (Right, Case DF) Deterministic hydrodynamic equations with fluctuating chemistry.

To illustrate effect of fluctuations on the growth of the labyrinth patterns we consider four models:

(FF) Fluctuating hydrodynamics with fluctuating chemistry
(DD) Deterministic hydrodynamics with deterministic chemistry
(FD) Fluctuating hydrodynamics with deterministic chemistry
(DF) Deterministic hydrodynamics with fluctuating chemistry

For the planar geometry, the number of species A particles per unit volume, $\rho Y_A/m_A$, at time t = 13,500 is presented

in Figs. 2 and 3. For fluctuating hydrodynamics with fluctuating chemistry (Case FF) the ensuing labyrinth patterns demonstrate no preferential alignment, except in the region corresponding to the initial stages of the propagation (see Fig. 2). For the deterministic hydrodynamic equations with deterministic chemistry (Case DD), the ensuing pattern is a stair-case, aligned normal to the direction of the propagating front. The labyrinth patterns are concentration maximas and minimas around the '+' state. Whereas the maximas are only $\sim$ 50% higher than the '+' state, the state immediately behind the leading concentration front can be much higher. For instance, since ρ = 5578, for the '+' state, ρY_A = 174.54; we note from Figs. 2 and 3 that the peak values for ρY_A are much higher (essentially the dark red regions immediately behind the propagating front). Thus, the concentration overshoots in the immediate vicinity of the front (like a concentration shock), and subsequently reaches maximas and minimas around the '+' state.

Fluctuations accelerate the propagation of the leading chemical wave front, with the fluctuating hydrodynamic scenarios (Cases FF and FD) being the fastest and the fully deterministic case (Case DD) being the slowest; Case DF (Deterministic hydrodynamic equations with stochastic chemistry) has a front speed between the two extremes. Furthermore, fluctuations allow a much wider variation of concentration within the labyrinth structures, with red, green and yellow colors observed within the structures in Case FF. By comparison, in Case DD the horizontal structures are all uniform in that they have the same concentration within each structure. In Fig. 3 we see that for Case DF, due to the absence of hydrodynamic fluctuations, the labyrinth structures are preponderantly biased normal to the direction of propagation of the front and are primarily red strips, indicating that the concentration variation within the structure is relatively lesser than Case FF.

We also observe in Figs. 2 and 3 that the labyrinth structures are more elongated for Case FF than the other cases; this is presumably due to the increased reaction-diffusion activity resulting when fluctuations are present as more mass (of any species) can now be transported over a wider spatial range. For deterministic hydrodynamics with fluctuating chemistry (Case DF in Fig. 3) the absence of hydrodynamic fluctuations produces "spots" immediately behind the leading front, from which the next generation of patterns will subsequently evolve. Such spots are not as evident for the other cases; thus, the pattern formation differs with and without hydrodynamic fluctuations.

The number of species A particles per unit volume, $\rho Y_A/m_A$, for the cylindrical Schlogl model at time t = 6500 is presented in Figs. 4 and 5. As before, the leading reaction front is the fastest for Cases FF and FD, slowest for Case DD, and in between for Case DF, highlighting the accelerating effect of fluctuations. For deterministic hydrodynamics with deterministic chemistry , we expect to observe concentric circles due to the absence of fluctuations, but due to the use of a cartesian grid to capture a circular front, we observe grid-related spurious artifacts (see Case DD in Fig. 4). As was the case for the planar front, here too the labyrinth patterns are longer when both hydrodynamic fluctuations are present (Cases FF and FD) and spots are observed in the patterns for Case DF.

CONCLUSIONS

We are accustomed to viewing the world as deterministic and this mechanistic point of view has been reinforced over and over by the technological successes of modern engineering. Yet this comfortable, predictable model cannot be applied to the microscopic world. At the molecular scale, the state of a fluid is uncertain and constantly changing. At hydrodynamic scales the probabilistic effects are not quantum mechanical but entropic in origin, that is, due to spontaneous, random fluctuations.

Directing Matter and Energy: Five Challenges for Science and the Imagination, a report by the Basic Energy Sciences Advisory Committee, contains the following insightful observation: "(Biological) evolution has embraced stochastic fluctuations and often relies on them for the functionality of the system. This suggests an interesting design principle that humans have not yet learned to use. Exploitation of statistical fluctuations may well be essential to accomplish some of the more exotic tasks living systems are able to perform . . . Realizing the promise of nanoscience requires that we deal with non equilibrium and fluctuations" [45].

Numerical modeling of hydrodynamic fluctuations has already yielded interesting, fundamental results observed in simple gases and this work is now being extended to complex multi-component fluids, including chemical reactions, where new phenomena are to be found. For example, Turing patterns are visibly different depending on relative contributions of hydrodynamic versus chemical fluctuations. For these studies Direct Simulation Monte Carlo and fluctuating hydrodynamics are complementary numerical methods and each holds the promise for significant future contributions in the field of nanofluidics.

REFERENCES

1. J. Eggers, *Phys. Rev. Lett.* **89**, 084502 (2002).
2. C. V. den Broeck, R. Kawai, and P. Meurs, *Phys. Rev. Lett.* **93**, 090601 (2004).
3. M. Wu, G. Ahlers, and D. S. Cannell, *Phys. Rev. Lett.* **75**, 1743–1746 (1995).
4. K. Kadau, C. Rosenblatt, J. L. Barber, T. Germann, Z. Huang, P. Carls, and B. J. Alder, *PNAS* **104**, 7741–7745 (2007).
5. A. Lemarchand, and B. Nowakowski, *Molecular Simulation* **30**, 773–780 (2004).
6. T. Butler, and N. Goldenfeld, *Phys. Rev. E* **84**, 011112 (2011).
7. A. Lemarchand, and B. Nowakowski, *Euro Phys. Lett.* **94**, 48004 (2011).
8. P. Dziekan, A. Lemarchand, and B. Nowakowski, *J. Chem. Phys.* **137**, 074107 (2012).
9. T. M. Squires, and S. R. Quake, *Rev. Mod. Phys.* **77**, 977 (2005).
10. E. Weinan, *Principles of Multiscale Modeling*, Cambridge University Press, 2011, ISBN 9781107096547, URL `http://books.google.com/books?id=9uTjKO2Ix-YC`.
11. G. A. Bird, *Molecular Gas Dynamics and the Direct Simulation of Gas Flows*, Clarendon, Oxford, 1994.
12. F. J. Alexander, A. L. Garcia, and B. J. Alder, *Phys. Fluids* **6**, 3854 (1994).
13. M. A. Gallis, *J. Microelectromechanical Systems* **13**, 653–659 (2004).
14. L. D. Landau, and E. M. Lifshitz, *Fluid Mechanics*, vol. 6 of *Course of Theoretical Physics*, Pergamon, 1959.
15. J. M. O. de Zarate, and J. V. Sengers, *Hydrodynamic Fluctuations in Fluids and Fluid Mixtures*, Elsevier Science, 2007.
16. J. B. Bell, A. L. Garcia, and S. A. Williams, *Phys. Rev. E* **76**, 016708–1–12 ((2007)).
17. A. Donev, E. Vanden-Eijnden, A. Garcia, and J. Bell, *CAMCOS* **5**, 149–197 (2010).
18. N. Hadjiconstantinou, A. L. Garcia, M. Bazant, and G. He, *J. Comput. Phys.* **187**, 274–297 (2003).
19. M. Tysanner, and A. L. Garcia, *J. Comput. Phys.* **196**, 173–183 (2004).
20. A. L. Garcia, *Comm. App. Math. and Comp. Sci.* **1**, 53–78 (2006).
21. H. S. Wijesinghe, and N. G. Hadjiconstantinou, *International Journal for Multiscale Computational Engineering* **2**, 189–202 (2004).
22. K. M. Mohamed, and A. A. Mohamad, *Microfluidics and Nanofluidics* **8**, 283–302 (2009).
23. J. B. Bell, J. Foo, and A. Garcia, *J. Comput. Phys.* **223**, 451–468 (2006).
24. S. A. Williams, J. B. Bell, and A. L. Garcia, *SIAM Multiscale Modeling and Simulation* **6**, 1256–1280 (2008).
25. A. Donev, J. B. Bell, A. L. Garcia, and B. J. Alder, *SIAM J. Multiscale Modeling and Simulation* **8**, 871–911 (2010).
26. M. M. Mansour, A. L. Garcia, G. C. Lie, and E. Clementi, *Phys. Rev. Lett.* **58**, 874–877 (1987).
27. A. Garcia, M. Mansour, G. Lie, M. Mareschal, and E. Clementi, *Phys. Rev. A* **36**, 4348–4355 (1987).
28. A. Donev, A. de la Fuente, J. B. Bell, and A. L. Garcia, *Phys. Rev. Lett.* **106**, 204501 (2011).
29. A. Donev, A. de la Fuente, J. B. Bell, , and A. L. Garcia, *JSTAT* **2011**, P06014 (2011).
30. V. Giovangigli, *Multicomponent Flow Modeling*, Birkhauser Boston, 1999.
31. A. Ern, and V. Giovangigli, *EGLIB: A general-purpose Fortran library for multicomponent transport property evaluation, Version 3.4*, 2004.
32. J. O. Hirschfelder, C. F. Curtiss, and R. B. Bird, *Molecular Theory of Gases and Liquids*, John Wiley and Sons, INC., New York, 1954.
33. L. Waldmann, *Transporterscheinungen in Gasen von mittlerem Druck, Handbuch der Physik XII*, Springer Verlag, Berlin, Gottingen, Heidelberg, 1958.
34. V. D. Valk, *Physica* **29**, 417 (1963).
35. K. Balakrishnan, J. B. Bell, A. Donev, and A. L. Garcia, *in preparation for Phys. Rev. E* (2012).
36. H. C. Ottinger, *The J. Chem. Phys.* **130**, 114904 (2009).
37. D. A. Bini, N. J. Higham, and B. Meini, *Numerical Algorithms* **39**, 349–378 (2005).
38. T. Poinsot, and D. Veynante, *Theoretical and Numerical Combustion*, R.T. Edwards, Inc., 2001.
39. D. T. Gillespie, *J. Chem. Phys.* **113**, 297 (2000).
40. D. T. Gillespie, *J. Chem. Phys.* **115**, 1716 (2001).
41. H. Salis, and Y. Kaznessis, *J. Chem. Phys.* **122**, 54103 (2005).
42. V. Sotiropoulos, M.-N. Contou-Carrere, P. Daoutidis, and Y. N. Kaznessis, *IEEE/ACM Transactions on Computational Biology and Bioinformatics* **6**, 470 (2009).
43. A. M. Turing, *Phil. Trans. R. Soc. Lond. B* **237**, 37 (1952).
44. F. Schlogl, *Z. Physik* **253**, 147 (1972).
45. B. E. S. A. Committee, Directing matter and energy: Five challenges for science and the imagination, Tech. rep., Dept. of Energy (2007).